THE SOLAR WIND AND JOVIAN DECAMETRIC RADIO EMISSION

By O. B. Slee* and C. S. Higgins*

[*Manuscript received February* 9, 1968]

Summary

Spaced-receiver observations of the 19·7 MHz radio emission from Jupiter during 1963 and 1964 demonstrate that many of the so-called bursts with quasi-periods of 1–10 sec are caused by the sweeping of an interplanetary diffraction pattern across the receiver by the motion of scattering irregularities in the solar wind. Measurements made on these scintillations include arrival time differences at spaced receivers, scintillation rate, angular position scintillation, and the width of the scattered angular power spectrum.

The derived properties of the scattering irregularities are as follows. (1) The solar wind is radially directed with respect to the Sun and possesses an average velocity $V_S \sim 600$ km sec^{-1}. (2) R.M.S. deviations in the magnitude and direction of V_S, averaged over considerable path lengths through interplanetary space, are less than 20% and 5° respectively. (3) The scale size of the irregularities in electron density is approximately 150 km. (4) The scattering is strong at 19·7 MHz for all directions in the ecliptic plane; the r.m.s. phase modulation varies from about 1 rad near opposition to about 11 rad at an elongation of 20°. (5) The conclusions in (3) and (4) are consistent with an r.m.s. electron density that varies with heliocentric distance R (a.u.) according to the relation $\{\overline{(\Delta N)^2}\}^{\frac{1}{2}} \sim 0{\cdot}2\,R^{-2}$ electrons cm^{-3}. (6) The irregularities in electron density with dimensions of hundreds of kilometres are relatively weak ($\sim 10\%$) in comparison with the average electron density.

Theoretical restrictions on source size are used to derive an upper limit of $\sim 0{\cdot}6$ sec of arc to the angular diameter of the decametric source on Jupiter. It is shown that the intensity scintillations are significantly reduced when the line of sight passes within 60° of the Sun; if this is due to the finite source size, a lower limit of $\sim 0{\cdot}1$ sec of arc can be assigned to the source diameter.

I. Introduction

Shortly after the discovery of the Jovian decametric radio emission by Burke and Franklin (1955) it was realized that some, if not all, of the intensity variations may be imposed on an essentially steady intrinsic emission by propagation effects between the planet and observer. Such considerations led Gardner and Shain (1958) to record bursts simultaneously at sites separated by 25 km, observations that showed the presence of considerable differences between the time variations at the two receivers. Subsequent spaced-receiver experiments by Smith *et al.* (1960) and Douglas and Smith (1961) over baselines varying in length from 15 to 7000 km showed that all degrees of burst correlation could be experienced; the differences were usually ascribed to the effects of ionospheric scintillations which, from discrete radio source observations, were known to be poorly correlated over distances greater than about 5 km.

* Division of Radiophysics, CSIRO, Box 76, P.O. Epping, N.S.W. 2121.

The valuable work of Douglas (1964) has been instrumental in changing our basic notions on the origins of the Jupiter bursts. Using receivers spaced at distances up to 100 km he was able to detect a systematic difference between the burst arrival times; this led to the conclusion that much of the burst structure is not an intrinsic property of Jupiter but is due to the movement of an interplanetary diffraction pattern across the Earth's surface.

Slee and Higgins (1963) began spaced-aerial observations over a 32 km baseline in 1962 with the primary object of performing angular size measurements of the burst sources using a radio-linked phase-sensitive interferometer. An essential part of the measurement was the recording of the total power signals received at the spaced aerials using receiving systems with almost identical characteristics. The experiment was continued on a more comprehensive scale during 1963 and 1964 with baselines extending from 17 to 200 km.

Some of the results of this experiment with emphasis on the angular size observations have been published by Slee and Higgins (1965, 1966). The present paper considers more aspects of the Jupiter burst phenomenon, including burst arrival times, burst rate, angular position scintillations, and apparent angular size, and uses the results to derive some useful information about the interplanetary diffraction patterns and the electron irregularities in the solar wind.

One important advantage of the Jupiter burst method of observing the interplanetary medium lies in its ability to detect the scattering effects with relatively unsophisticated receivers and physically small aerial systems over a large range of heliocentric distances close to the ecliptic plane; this is brought about by the fortunate circumstance that Jupiter happens to be a very powerful low frequency radio source of very small angular dimensions. There are, however, a few disadvantages of this technique when compared with corresponding observations made with the extragalactic radio sources of very small angular size, generally at much higher frequencies. Firstly, the Jupiter decametric transmission appears to be inherently intermittent, with the result that one is limited to relatively short samples of the diffracting properties of the solar wind; typically, with a fixed receiving aerial at 20 MHz one could expect to see the Jupiter bursts for 1 hr every 3 days. Secondly, investigations of the interplanetary medium are limited to those regions close to the ecliptic plane. Finally, another element of uncertainty is introduced into the interpretation of the diffraction patterns in terms of the physical parameters of the solar wind by the fact that the source is located at a finite distance behind the diffracting irregularities; this results in the application of a generally unknown magnification factor to the diffraction scale size and pattern velocity. However, this may not be as disadvantageous as it first appears, since a comparison of these measurements from both Jupiter and extragalactic source observations should result in a determination of the magnification factor and hence of the location of the effective diffracting region along the line of sight.

The scheme of the present paper is as follows. In Section II the long baseline equipment and observational techniques are described, while Section III discusses the general appearance of the present Jupiter records and in particular the burst correlation at separated sites. Section IV introduces some relevant aspects of the

diffraction theory, the results of which will be used to derive approximate physical characteristics for the scattering irregularities using their observed effects on the radiation reaching the ground. In Section V we demonstrate the validity of our measurements of the relative burst arrival time differences, which we then use to deduce the drift velocities of the diffraction patterns. Section VI introduces the topic of burst rate, which is shown to change systematically with Jupiter's elongation and to provide additional information on the pattern velocities. Section VII discusses the methods available for measuring the diffraction scale and deduces numerical values for a number of events. The question of the phase deviations associated with the amplitude scintillations is treated in Section VIII and measurements of the interferometer fringe phases are used to show that the r.m.s. phase deviations are also dependent on Jupiter's elongation. Finally, in Section IX, we attempt to use this information and that from other related experiments to deduce the physical state and dynamics of the solar wind.

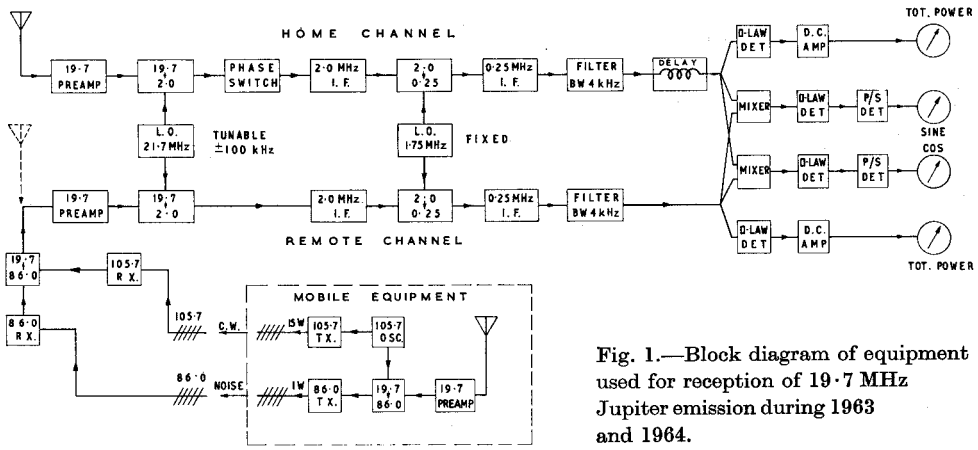

Fig. 1.—Block diagram of equipment used for reception of 19·7 MHz Jupiter emission during 1963 and 1964.

II. Equipment and Observational Techniques

Figure 1 is a block diagram of the equipment at both the remote and home site ends of the baseline; it excludes the power supplies, noise-diode calibrators, and pulse generation circuits. It consists basically of two double conversion superheterodyne receivers that use common local oscillators, the first being tunable over a band of ± 100 kHz. Considerable attention was directed to the tuning of the two 4 kHz bandwidth filters which ultimately determine the centre frequencies and bandpasses of the receivers. The square-law detectors, phase-sensitive detectors, d.c. amplifiers, and chart recorders had identical gain and response time characteristics, so that for all practical purposes the responses of the two receivers were closely the same. The equipment at the remote site was mobile and included a 19·7 MHz preamplifier of 150 kHz bandwidth. Its output was upconverted to 86·0 MHz and transmitted, together with the 105·7 MHz c.w. upconversion signal, to the home site, where the noise signal was reconverted coherently to 19·7 MHz. Using transmitting and

receiving Yagi aerials, with power gains of about 10, it was found that transmitted powers of 1·5 W r.m.s. noise and 15 W c.w. were sufficient to ensure signal to noise ratios in excess of 100/1 at the final detector output. At the shorter spacings these power levels were high enough to saturate the receivers, so that it was found necessary to insert attenuators in the radio-link receiving system; these were adjusted to ensure that approximately the same powers were delivered to the radio-link receivers on all spacings.

The overall noise figures of the two channels were about three in power, but of course in operation the effective noise figures were determined by the high cosmic background temperature of about 50 000°K. Identical high power noise diodes were located at each end of the baseline and were used to perform total power calibrations by injecting random noise up to twice the cosmic background level. The calibration from the remote site was recorded at the home site and hence calibrated the complete remote channel. In addition to calibrating the total power channels, we were able to check the gains of the interferometer mixing and phase-sensitive detector circuits by modulating the noise diodes with a square wave of the phase-switching frequency; this was achieved by generating the phase-switching frequency at the remote site and transferring it to the home site in the form of a pulse modulation on the 105·7 MHz reference signal. Artificial fringes were then generated and recorded on the phase-sensitive channels by phase sweeping the phase-sensitive detector reference waveform with respect to the phase-switched output. Both remote and home channels were gain controlled to preset levels by means of independent automatic gain control systems having time constants of 60 sec.

Two parallel recording systems were available; the arrangement most often used consisted of two double-pen chart recorders of full-scale response time $0^s{\cdot}5$ operating at a chart speed of 76 mm min^{-1} giving the required two total power and two phase-sensitive (sine and cosine Fourier component) records. An alternative system for the shorter duration bursts consisted of a four-pen chart recorder of full-scale response time $0^s{\cdot}02$ operating at a chart speed of 254 mm min^{-1}. These chart speeds were found adequate to resolve the majority of the burst structure and to provide a reasonable spacing for the interference fringes, even on the longest baseline.

A number of aerial configurations were used over the 2 yr recording interval; the usual arrangement was two pairs of $\lambda/2$ horizontally polarized dipoles at each site with one pair orientated with axes north-west–south-east and the other pair rotated by 90°, a configuration that allowed observation of Jupiter for up to 8 hr near upper transit. The dipoles in each pair were parallel and spaced $\lambda/4$ to $\lambda/2$ above ground and so phased as to achieve maximum response at the midpoint of the hour-angle coverage of each dipole. At the home site the aerial arrays were duplicated so that the radio link could be disconnected and the outputs of two aerial arrays spaced only a few metres apart could be applied to the home equipment in order to obtain a zero baseline reference point for the angular size measurements.

During the observing interval we used the three baselines shown in Figure 2, which is a map of that part of eastern Australia within a few hundred kilometres of

Sydney. The baselines were of lengths 17·4, 85·5, and 200·0 km respectively and were orientated generally in a north-northeast–south-southwest direction; this coincided with the direction of the relatively flat coastal plain bordered on one side by a mountain range with peaks up to 1600 m above sea level and on the other by the Pacific Ocean. By placing our extreme southern and northern sites on relatively high (750 m) outcrops of this mountain range, we achieved line-of-sight transmission across the coastal plain for the radio links.

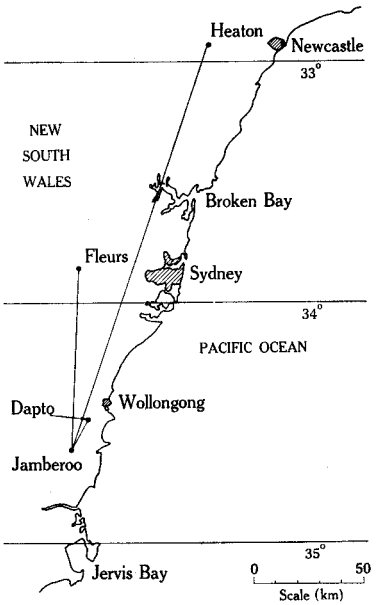

Fig. 2.—Sketch map of the eastern Australian coast near Sydney showing the locations of the receiving sites used during the Jupiter long baseline experiment. The home site was situated at Jamberoo.

Both the home and remote stations were manned during a Jupiter observation, since it was necessary to perform noise-diode calibrations at both sites before and after each recording session, which typically lasted about 8 hr. Our observations were confined to the interval 2300 to 0700 hr local time. The former limit was imposed on us by the fact that our radio link operated within the television bands, so that we could neither transmit nor receive during the normal television service hours. Observations usually ceased at dawn because of the rapidly increasing level of interference. This asymmetry in the observations with respect to local midnight resulted, unfortunately, in an almost complete lack of data after opposition during the apparitions of both 1963 and 1964.

Because of the difficulties of manning simultaneously two stations, often in rather remote mountain areas, we confined our observations to those nights on which there was a reasonable probability of Jupiter decametric emission during the observing period; these nights, usually two or three weekly, could be predicted from the published statistical data on the probability of burst occurrence as a function of Jupiter's system III longitude.

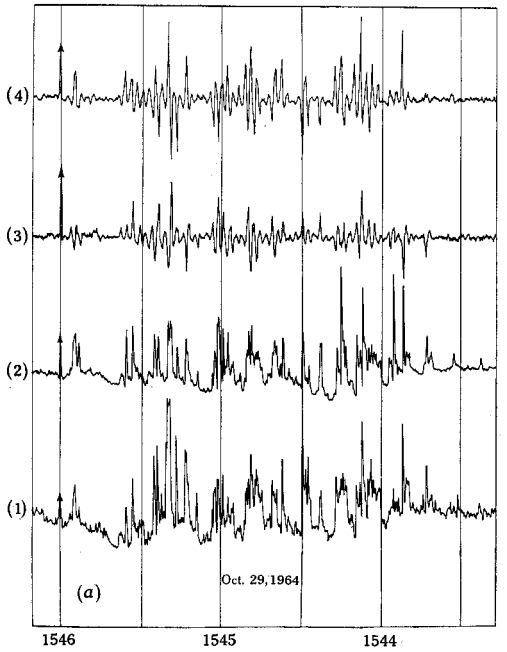

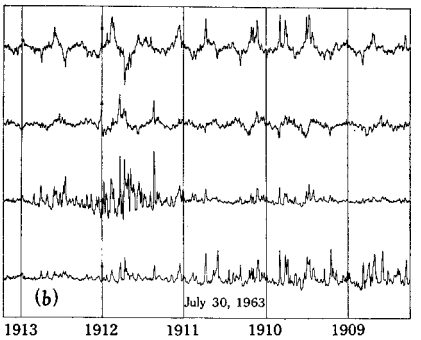

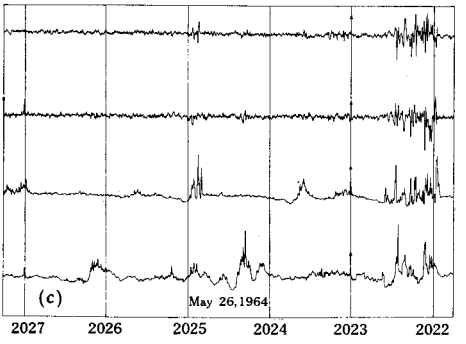

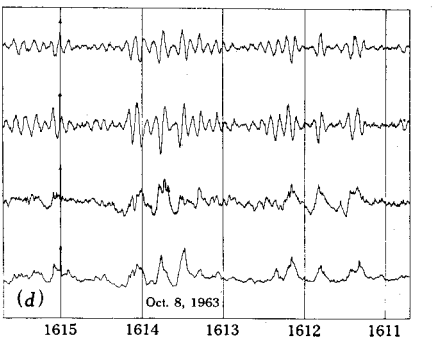

Universal time

Fig. 3.—Examples of 19·7 MHz chart recordings obtained during the long baseline observations. The four traces in each figure refer respectively to (from the bottom): (1) total power from the outstation; (2) total power from the home station; (3) and (4) sine and cosine components of the interference pattern. At times of strong Jovian emission the automatic gain control produces a depression of the baselevel which is noticeable on some of the total power traces.

(*a*) Section of noise storm showing good correlation between burst amplitudes at sites 200 km apart. Regular fringes of correct period are also present.

(*b*) Recording showing poor amplitude correlation between bursts received at sites 85·5 km apart. The differences are due to uncorrelated ionospheric scintillations that vary the relative amplitudes at a slow rate but leave the individual Jovian bursts with similar relative shapes. The ionospheric scintillations are not appreciably perturbing the phase of the interferometer pattern.

(*c*) Portion of a noise storm recorded when Jupiter was 26° from the Sun, showing the characteristic poor correlation in amplitude and shape between bursts recorded at sites 85·5 km apart. Note the irregular nature of the fringes as compared with (*a*), (*b*), and (*d*).

(*d*) Bursts recorded over the 85·5 km baseline near opposition, showing the characteristic longer durations. The bursts at the separated sites possess similar shapes and give rise to fringes with a high degree of regularity.

III. Appearance of Recordings

Figure 3(*a*) shows a short section of a Jupiter noise storm recorded over the 200 km baseline. The four chart recordings normally taken at the home site have been carefully traced and aligned in time as accurately as possible. Beginning at the bottom of the figure, the fourth trace is a total power record of the bursts received at the remote station and transmitted to the home site over the radio link; the third trace shows the corresponding total power recording of the bursts arriving at the home site. The upper two traces show the sine and cosine Fourier components of the interferometer pattern formed by multiplying the signals in a phase-switched system.

The degree of correlation between the total power channels of Figure 3(*a*) is probably close to the highest observed over our long baselines, although there were probably some slightly better examples on the shorter 85·5 km spacing. This high degree of correspondence between burst shapes and amplitudes was, however, not usually maintained for long intervals of time; after perhaps 10 min of such recording the correlation would sometimes deteriorate to the situation shown in Figure 3(*b*). Here close inspection shows that although the individual bursts are present at both sites, their relative amplitudes can be markedly different. It would appear that the Jovian burst amplitude is here being deeply modulated at a relatively low frequency by completely uncorrelated ionospheric scintillations at the two sites. The short sections of record shown in Figures 3(*a*) and 3(*b*) are extreme cases and more often a degree of correlation intermediate between the two would be present.

In addition to burst amplitude decorrelation we have obtained some recordings in which there are relative changes on a time scale much shorter than the normal ionospheric scintillation periods of 30–60 sec. These changes take place within periods of a second or so and hence destroy the correspondence between individual burst shapes. Such a condition exists on the recordings shown in Figure 3(*c*), which applies to observations made when Jupiter was only 26° from the Sun; similar recordings were obtained on all six occasions in 1964 when bursts were observed while Jupiter was less than 50° from the Sun. Attention is also directed to the high degree of irregularity in the interferometer fringes, characteristic of this type of record.

In contrast to the high burst rate and general irregularity of fringes depicted in Figure 3(*c*), the much slower burst rate and high regularity of fringes characteristic of our recordings near opposition are shown in Figure 3(*d*); the typical appearance of bursts in groups, each of about 60 sec duration, is evident on these traces.

Measurements of burst arrival time differences at separated sites were necessarily restricted to those relatively infrequent occasions on which the total power recordings were well correlated in amplitude and shape; however, we were not necessarily restricted to the use of such highly correlated records as shown in Figure 3(*a*), since the presence of moderately intense ionospheric scintillations resulted only in rather slow relative intensity changes which did not affect our ability to identify the same bursts on the two total power traces. As Figure 3(*c*) shows, interferometer fringes could be recorded even at times of poor burst shape and amplitude correlation so that measurements of angular size and angular position are practicable for most portions of a Jupiter noise storm.

IV. Some Relevant Aspects of the Diffraction Theory

In this discussion it is assumed that the irregularities in refractive index that are responsible for the scattering are isotropic, so that the one-dimensional forms of the functions describing the complex amplitude of the radio wave and its autocorrelation coefficient across any plane transverse to the direction of propagation will be satisfactory.

The existing theory assumes that the irregularities are confined to a short section of the path between the source and observer. This ensures that, while the wave is in the scattering region, the variations in complex amplitude are composed only of phase fluctuations. The one-dimensional complex amplitude of the wave is defined by the equation

$$\mathbf{f}(x) = A(x) \exp\{\mathrm{i}\phi(x)\}, \tag{1}$$

where $A(x)$ and $\phi(x)$ are respectively the real amplitude and phase distributions across a plane transverse to the direction of propagation.

In the diffraction process of interest here, $\mathbf{f}(x)$ is a random function and its spatial variations across any transverse plane are conveniently described by its autocorrelation function

$$\rho_f(\xi) = \frac{[\mathbf{f}(x)\,\mathbf{f}^*(x+\xi)]_{\mathrm{av}} - \{[\mathbf{f}(x)]_{\mathrm{av}}\}^2}{[\mathbf{f}(x)\,\mathbf{f}^*(x)]_{\mathrm{av}} - \{[\mathbf{f}(x)]_{\mathrm{av}}\}^2}, \tag{2}$$

where the averages are taken over all values of x. The correlation functions for the real amplitude, intensity, and phase fluctuations are defined in a similar way.

(a) *Mean Square Phase Modulation* ϕ_0^2

Bramley (1954) has investigated the theory of scattering in an extended medium in which the scale sizes and electron contents of the irregularities are statistically similar for all samples of the region. It is assumed that the values of electron density are normally distributed and that their spatial distribution is described by an isotropic Gaussian autocorrelation function, $\rho_{\Delta N}(r) = \exp(-r^2/L^2)$, where L is the scale size. The resulting complex amplitude across a plane immediately below the diffracting region consists of a real amplitude that is independent of x and a phase $\phi(x)$ with a normal distribution of phase deviations having the mean square value

$$\phi_0^2 = (\pi^4 e^4 \lambda^2 / m^2 c^4)\, LZ\, \overline{(\Delta N)^2}, \tag{3}$$

where $\overline{(\Delta N)^2}$ is the mean square deviation of electron density, e and m are the electronic charge and mass, λ is the wavelength of the radio wave, and c is the velocity of light.

If the properties of the scattering medium vary as the wave propagates through it, that is, L and $\overline{(\Delta N)^2}$ are functions of Z, it appears legitimate to subdivide the region into a series of thin slabs, each of which contributes a mean square phase

deviation given by equation (3). The total mean square phase deviation is then computed by summing the separate contributions so that

$$\phi_0^2 = \frac{\pi^4 e^4 \lambda^2}{m^2 c^4} \int_Z L(Z)\, \overline{[\Delta N(Z)]^2}\, \mathrm{d}Z\,. \tag{4}$$

(*b*) *Angular Spectrum of Scattered Radiation*

A bundle of parallel rays from a distant point source is scattered into a cone with axis corresponding to the original direction of propagation and semi-opening angle dependent upon the scale and strength of the irregularities in electron density. The angular power spectrum $|\,\mathbf{F}(S)\,|^2$ and autocorrelation function $\rho_f(\xi)$ are Fourier transforms of each other and are independent of the distance from the diffracting region. Hence, although the complex amplitude changes with distance, a measurement of its autocorrelation function or angular power spectrum on the ground plane is sufficient to define the spatial distribution of $\mathbf{f}(x)$ over a plane directly below the scattering region.

The relationship of $\rho_f(\xi)$ and $|\,\mathbf{F}(S)\,|^2$ to the scale size of the electron irregularities in the diffracting region has been presented rather clearly by Ratcliffe (1956). If the irregularities possess a Gaussian autocorrelation function

$$\rho_{\Delta N}(r) = \exp(-r^2/L^2)\,,$$

then the autocorrelation function for the complex amplitude is of the form

$$\rho_f(\xi) = \exp(-\xi^2/\xi_0^2)$$

and the angular power spectrum is described by

$$|\,\mathbf{F}(S)\,|^2 = \exp(-S^2/S_0^2)\,.$$

The relationships between the scale sizes L, ξ_f, and S_0 depend upon the strength of the scattering:

(i) *Weak Scattering*, $\phi_0^2 \ll 1\ \mathrm{rad}^2$

$$S_0 = \lambda/\pi L\,, \qquad \xi_f = L\,. \tag{5}$$

(ii) *Strong Scattering*, $\phi_0^2 \geqslant 1\ \mathrm{rad}^2$

$$S_0 = \phi_0(\lambda/\pi L)\,, \qquad \xi_f = L/\phi_0\,. \tag{6}$$

It is of interest to note that the width of the angular power spectrum increases in proportion to λ for weak scattering, but as λ^2 for strong scattering. In addition, S_0 in equations (5) describes the half-width to $\exp(-1)$ of a relatively weak halo surrounding a bright undeviated component; for strong scattering most of the incident power is scattered into a spectrum whose half-width is measured by S_0 in equations (6).

The determination of ξ_f or S_0 involves measurements of both the real amplitude and phase distributions across the ground plane. This is most conveniently performed

by means of a phase-sensitive interferometer with variable spacing between the aerials. Ratcliffe (1956) has demonstrated that the fringe visibility function $V(\xi)$ is identical with $\rho_f(\xi)$. Hence the spacing of the interferometer aerials for which the fringe visibility has been reduced to $\exp(-1)$ is a measure of ξ_f.

(c) *Interferometer Measurements of* ϕ_0^2

It is important to develop an experimental method of estimating the mean square phase modulation. Not only does a knowledge of ϕ_0^2 allow a determination to be made of the so-called scattering function,

$$\int_Z L(Z)\ \overline{[\Delta N(Z)]^2}\,\mathrm{d}Z,$$

given by equation (4) but also, for strong scattering, its value is needed before the scale size of the electron irregularities can be deduced from the interferometer measurements of the angular power spectrum.

The phase of the interferometer fringes undergoes random changes that are related to the value of ϕ_0^2. For a distant source, the mean square phase difference $\overline{(\Delta\phi)^2}$ between the signals at the spaced receiving sites (the quantity measured from the displacements of the fringes from their unperturbed positions) is given by

$$\overline{(\Delta\phi)^2} = 2\{1-\rho_\phi(\xi)\}\phi_0^2, \tag{7}$$

where $\rho_\phi(\xi)$ is the autocorrelation function for the phase deviations across the ground.

It may be thought that a lack of knowledge of $\rho_\phi(\xi)$ would prevent a determination of ϕ_0^2 from the measured value of $\overline{(\Delta\phi)^2}$. However, the approximate scale length of the phase fluctuations is known from the measurements of the complex amplitude scale; in addition, provided the interferometer spacing is long enough to ensure that the phase fluctuations are not highly correlated then the exact value of $\rho_\phi(\xi)$ is not important, since under these conditions $\overline{(\Delta\phi)^2} \to 2\phi_0^2$.

(d) *Intensity Fluctuations across the Ground Plane*

Interference between the components of the angular spectrum at the ground plane gives rise to a distribution of real amplitude $A(x)$. Previous experiments with interplanetary scintillations have been limited to obtaining a measure of the distribution of intensity $A^2(x)$, which is assumed to be adequately specified by its mean square fluctuation and a Gaussian autocorrelation function

$$\rho_{A^2}(\xi) = \exp(-\xi^2/\xi_0^2).$$

The distance along the ground ξ_0 for which the correlation is reduced to $\exp(-1)$ is known as the scale length of the intensity fluctuations.

Bramley and Young (1967) have derived some general results for the diffraction of a plane wave by a phase-changing screen containing irregularities with a Gaussian autocorrelation function. For strong scattering ($\phi_0^2 \geqslant 1$), the case that is of greatest

interest in these observations, the intensity fluctuations across the ground plane at distance Z from the diffracting region are fully developed when

$$2\lambda Z/\pi L^2 \geqslant 1\,. \tag{8}$$

The scale length of the intensity fluctuations varies considerably, but with $\phi_0^2 \geqslant 1$ and equation (8) satisfied so that the observer is in the Fraunhofer region

$$\xi_0 = L/\sqrt{2}\,\phi_0\,. \tag{9}$$

(e) *Effect of Spherical Wave Front*

Ratcliffe (1956) and Pisareva (1958) have discussed the case of an observer and point source distant Z_1 and Z_2 respectively from the diffracting screen. They show that the actual distance should be replaced by an equivalent distance $Z = Z_1 Z_2/(Z_1+Z_2)$ and the problem treated in the same manner as that of a point source at infinity.

One of the more important consequences of this modification to the theory is the increase in the scale of the diffraction patterns relative to those for an incident plane wave. The scale lengths for both the complex amplitude and intensity variations across the ground are increased by the factor $(Z_1+Z_2)/Z_2$.

(f) *Finite Angular Size of Source*

Little and Hewish (1966) have shown that the mean square intensity fluctuation due to a source of finite angular size is less than that from a point source. Provided the observer is in the Fraunhofer region so that equation (8) is satisfied, the r.m.s. intensity fluctuation has been reduced to half that of a point source when

$$\xi_0/Z\psi_0 \approx 1\,, \tag{10}$$

where ξ_0 is the scale length for the intensity fluctuations, Z is the distance to the scattering region, and ψ_0 is the angular radius of the source to $\exp(-1)$.

(g) *Measurements of ξ_0 by the Method of the Drifting Pattern*

This method relies on a knowledge of the drift velocity V of the intensity diffraction pattern across the ground; the velocity may be computed from measurements of the differences between the arrival times of diffraction peaks at two or more points on the ground within the scale length ξ_0.

If the diffraction pattern remains relatively unchanged as it drifts, the observations of the temporal autocorrelation function $\rho(\tau)$ at one of the receivers can be converted into a spatial autocorrelation function $\rho_A{}^2(\xi)$ by writing $\xi = V\tau$. Often, to avoid the difficulties of performing the autocorrelation analysis on analogue recordings, it is more convenient to measure the average time interval $\bar{\tau}$ between the arrival of successive diffraction peaks. This yields the average distance $V\bar{\tau}$ between diffraction peaks, which is shown by Ratcliffe (1956) to be related to ξ_0 by the expression

$$\xi_0 = (2\cdot 6)^{-1}\, V\bar{\tau}\,. \tag{11}$$

(*h*) *Limitations of Thin Screen Theory*

For Jovian decametric observations it appears that the requirements of the existing diffraction theory may not be satisfied. Both the source and observer are embedded in the solar wind, whose scattering properties will, no doubt, vary considerably along the line of sight.

The application of equation (8), with $\lambda = 15$ m and $L = 150$ km, to a thin slab of the diffracting medium shows that amplitude fluctuations are well developed within a distance of 0·1 a.u. Under these conditions, successive slabs of the solar wind are illuminated by waves possessing spatial variations of amplitude as well as phase; there is, as yet, no theoretical solution of such a problem. Nevertheless, there are good reasons for believing that the electron content of the irregularities in the solar wind changes rapidly with heliocentric distance, with the result that a relatively short section of the path contributes most of the scattering. Consequently, it appears probable that deductions about the scale length, electron density, and velocity of the irregularities based on the thin screen theory are at least qualitatively correct.

V. Time Shifts between Bursts at Separated Sites

We have examined our recordings closely for periods of good total power correlation, with the result that we have selected 12 storms from a total of 39 for burst arrival time measurements.

The measurements were made by identifying a common fine structural feature for each burst event on the two total power records; the displacements of this feature from the nearest convenient time marks were then measured with an accurately graduated ruler to $\pm 0{\cdot}1$ mm. This procedure was repeated for every well-correlated burst recorded in the noise storm. In practice, after the measurement of the selected structural detail on one trace, the same feature was measured on the other, thus ensuring that the ruler zero was set independently for each burst.

The differences between the pairs of measurements were then subjected to a statistical test aimed at determining whether bursts for the storm as a whole showed a systematic tendency to arrive first at one site or the other. To do this the statistic chi-squared (χ^2), associated in this case with one degree of freedom, was calculated on the hypothesis that equal numbers of time shifts of both signs could be expected by chance. Table 1 summarizes the conclusions as to the validity of the measured time displacements. It can be seen that for 10 of the 12 storms, the value of χ^2 is significantly higher than would be expected for a random distribution of burst arrival time differences. Figure 4 shows several delay histograms that depict more clearly the distribution of measured time shifts on four of these occasions; it is apparent that the distributions are approximately Gaussian, so that their average values and r.m.s. dispersions provide meaningful information. The average time displacements $\overline{\Delta t}$ and their r.m.s. errors are listed in column 4 of Table 2. On all occasions except August 31, 1964 the bursts were received first at the north-east end of the baseline.

TABLE 1

VALIDITY OF TIME DIFFERENCES

Date of Observation	Total Measurable	Number of Bursts: Time Shift of S. Station relative to N. Station* +	−	0	χ^2 †
1963 Sept. 7	35	7	20	8	8·08
9	55	4	41	10	37·20
Oct. 8	47	13	31	3	7·85
1964 July 13	43	20	15	8	0·90
23	33	7	19	7	7·00
28	47	10	30	7	5·88
Aug. 4	70	19	32	19	4·53
11	23	4	19	0	9·80
31	61	39	16	6	10·65
Sept. 24	96	42	37	17	1·50
Oct. 18	60	7	51	2	34·40
29	121	23	78	20	35·80

* +, Burst arrival earlier at southern station; −, burst arrival later at southern station; 0, no difference.

† Calculated by apportioning the "0" shift number to the other two categories so as to preserve the existing ratios. χ^2 would exceed 3·84 by chance in 5% of similar trials and 6·63 in 1% of similar trials.

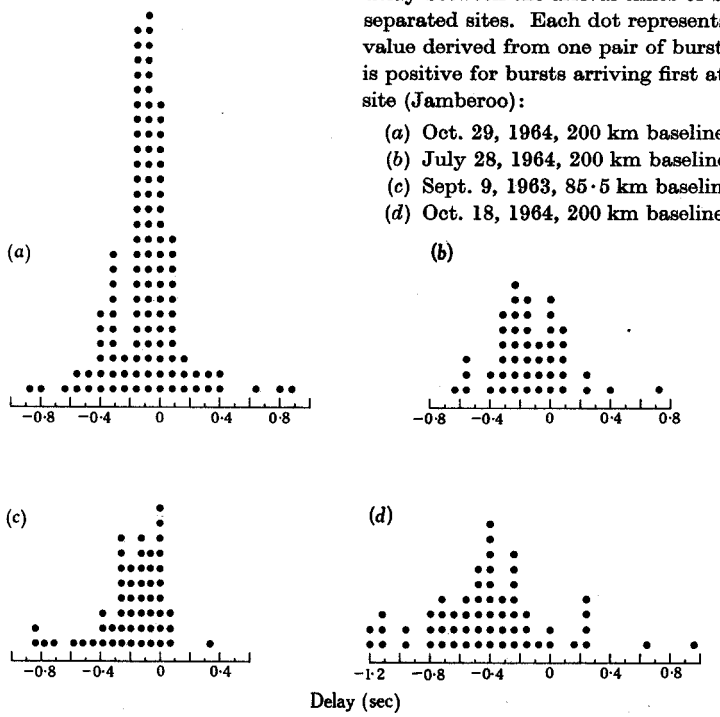

Fig. 4.—Histograms of the measured values of delay between the arrival times of bursts at separated sites. Each dot represents the delay value derived from one pair of bursts. The delay is positive for bursts arriving first at the home site (Jamberoo):

(*a*) Oct. 29, 1964, 200 km baseline
(*b*) July 28, 1964, 200 km baseline
(*c*) Sept. 9, 1963, 85·5 km baseline
(*d*) Oct. 18, 1964, 200 km baseline

The existence of systematic differences in burst arrival times at separated receivers suggests that much of the fine structure in Jovian bursts is not due to the emission mechanism but rather is imposed on the radiation during propagation. Such effects can be produced by a nonuniform distribution of radio brightness that drifts across the Earth's surface with a well-defined velocity. There is good evidence from the analysis of spaced-receiver observations of Jupiter by Douglas and Smith (1967) that the source of such brightness fluctuations lies in the diffracting properties of electron irregularities in the solar wind; the velocity of the latter is responsible for the transport of the resultant diffraction patterns across the Earth's surface.

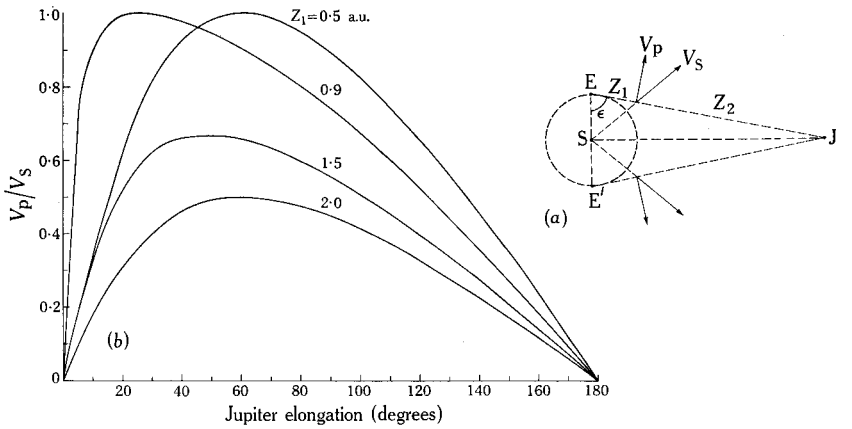

Fig. 5.—Geometry of the scattering problem in the ecliptic plane, assuming a radial solar wind V_S, is shown in (*a*). The Sun is at S, the Earth at E, and Jupiter at J; Z_1 and Z_2 are the distances to the diffracting layer from the Earth and Jupiter respectively, and V_p is the component of the solar wind transverse to the line of sight at the diffracting layer. The curves in (*b*) show the ratio V_p/V_S as a function of elongation and distance Z_1.

It is apparent that the velocity vector associated with a drifting pattern cannot be determined from observations over a single baseline. If, however, it is assumed that the diffraction takes place in a radially directed solar wind, thus specifying the direction of drift with respect to the baseline, the observed time displacements can be used to compute the magnitude of the velocity of the pattern. The geometry of the proposed model is shown in Figure 5, which illustrates how V_p, the transverse component of a radial solar wind V_S, would depend on both the elongation of the planet and the distance along the line of sight to the effective diffracting region. Except for the few days near opposition and conjunction when the small angle between the orbital planes of the Earth and Jupiter produces some important modifications and minor departures of the solar wind from purely radial motion may be important, V_p will be aligned approximately along the projection of the ecliptic on the plane perpendicular to the line of sight.

In order to use our measured time displacements for velocity computations, we have for each of the occasions listed in Table 2 projected both the ecliptic and baseline onto the plane perpendicular to the line of sight and computed the included angle θ; the average values of θ for each Jovian noise storm are given in column 3

of Table 2. The average velocity of the diffraction pattern across the plane perpendicular to the line of sight at the Earth, $\overline{V}'_{\mathrm{p}}$, was then obtained from the expression

$$\overline{V}'_{\mathrm{p}} = (S \cos \theta)/\overline{\Delta t},$$

where S is the spacing between receivers, $\overline{\Delta t}$ is the average arrival time difference, and it is assumed that the drifting brightness distributions are approximately circular. Values of $\overline{V}'_{\mathrm{p}}$ were deduced by this method on 10 occasions and are listed in column 5 of Table 2.

TABLE 2

MEASURED PARAMETERS OF DIFFRACTION PATTERNS

Elongation of Jupiter ϵ, average angle between baseline and ecliptic θ, average relative time shift $\overline{\Delta t}$, corrected average drift velocity of diffraction pattern $\overline{V}'_{\mathrm{p}}$, average burst spacing $\bar{\tau}$, average intensity of diffraction scale $\bar{\xi}_0$

(1) Observation Date	(2) ϵ (deg)	(3) θ (deg)	(4) $\overline{\Delta t}$ (sec)	(5) $\overline{V}'_{\mathrm{p}}$ (km sec^{-1})	(6) $\bar{\tau}$ (sec)	(7) $\bar{\xi}_0$ (km)
1963* Sept. 7	146	101·4	0·08±0·04	204	4·43±0·02	348
9	148	109·0	0·19±0·03	148‡	3·80±0·02	216‡
Oct. 8	179	116·5	0·34±0·10	111‡	7·66±0·06	327‡
1964† July 23	69	111·8	0·11±0·04	675‡	1·86±0·01	483‡
28	73	86·0	0·13±0·04	109	1·69±0·01	71
Aug. 4	79	97·2	0·09±0·02	288	1·60±0·01	177
11	85	112·5	0·22±0·06	344‡	2·03±0·01	269‡
31	103	87·0	0·20±0·04	54	2·09±0·01	44
Oct. 18	151	136·4	0·41±0·05	356‡	4·36±0·02	597‡
29	163	141·0	0·11±0·02	1410‡	1·45±0·01	785‡

* Baseline length 85·5 km, azimuth 5° east of north.

† Baseline length 200·0 km, azimuth 21° east of north.

‡ R.M.S. error unlikely to exceed 30%.

The errors involved in these determinations of $\overline{V}'_{\mathrm{p}}$ are comparatively large and come from two sources: (1) errors in $\overline{\Delta t}$, and (2) errors in θ due to departures of the solar wind from the radial direction. The random component of (1) due to the effects of noise and reading errors has been estimated from the dispersion displayed by individual values of Δt about the mean value for the storm; the r.m.s. errors in the values of $\overline{\Delta t}$ ranged from 12 to 50% with an average of 26%. In addition to the random component, there may at times be significant systematic errors, which are largely unknown. For example, the extremely high value of $\overline{V}'_{\mathrm{p}}$ for October 29, 1964 is probably due to a systematic underestimation of Δt because of the disturbing effects of s-pulses, which have been shown by Slee and Gent (1967) to be unconnected with the interplanetary medium. Errors due to (2) cannot be calculated with precision, but a consideration of the dispersion in burst rate described in Section VI suggests that the solar wind direction does not vary by more than $\pm 5°$ from the radial direction, so that θ is not likely to be in error by more than 5°. Unfortunately, the use of approximately north–south baselines in this experiment has resulted in generally large values of θ so that $\cos \theta$ is a rapidly varying function. However, the values of

$\overline{V}_p'$ indicated by a double dagger in Table 2 were obtained at hour angles for which an error in θ of 5° would give rise to an error in $\cos\theta$ of less than 23%. Consequently, combining the random components of (1) and (2), the r.m.s. errors in the more accurate values of $\overline{V}_p'$ in Table 2 should be less than 35%.

In order to derive the magnitude of the solar wind velocity from these measurements, the values of $\overline{V}_p'$ are first transformed to values of $\overline{V}_p$, the transverse velocity in the diffracting region, by multiplying by the reciprocal of the magnification factor (see Section IV). Then by the use of the curves in Figure 5 the solar wind velocity V_S may be estimated. It turns out that this computation is relatively insensitive to the distance to the equivalent diffracting screen because the magnification factor changes with Z_1 in such a way as to largely cancel the change in the ratio V_p/V_S.

The more reliable measurements of $\overline{V}_p'$ in Table 2, neglecting those obtained near opposition and the extremely high value of October 29, 1964, have been used to derive an average value for the solar wind. This is found to be $V_S = 630$ km sec^{-1} for a diffracting layer at $Z_1 = 1$ a.u. or $V_S = 560$ km sec^{-1} for a layer at 0·5 a.u.

VI. Burst Rates

The average time interval $\bar{\tau}$ between the reception of successive diffraction peaks at a fixed location on the Earth's surface can provide supplementary information about the average drift velocity of the diffraction pattern. The burst rates were

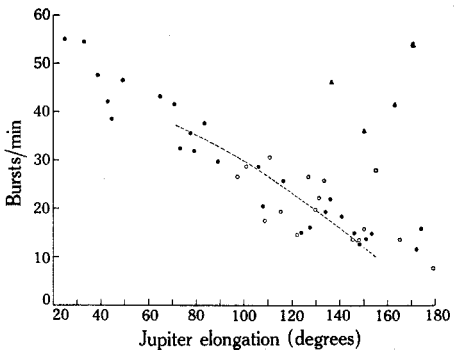

Fig. 6.—Nightly average values of burst rate plotted as a function of Jovian elongation. The open and full symbols refer respectively to measurements in 1963 and 1964. The triangular symbols represent the burst rates on nights during which a pronounced millisecond component (s-pulses) was detected. The dashed curve is described in the text.

measured by counting the diffraction peaks within time intervals that were kept short enough to embrace only those times of obvious burst activity with characteristic durations of between 30 and 60 sec. Typically, some 15–20 samples of burst rate were measured for each active night for which were calculated a sample average with an r.m.s. uncertainty of about 4%.

Figure 6 shows the nightly average values of burst rate plotted as a function of Jupiter's elongation; it includes data from 1963 (open symbols) and 1964 (full symbols). The four values represented by triangles were obtained during Jovian emission that contained considerable numbers of the relatively uncommon millisecond pulses (s-pulses) recognized from their characteristic "spitting" sounds in the loudspeaker. If the results from the s-pulses are ignored, the average burst rate increases systematically from about 10 min^{-1} near opposition to 55 min^{-1} at an

elongation of 25°. This trend is illustrated in the chart recordings of Figure 3, in which Figure 3(*d*) shows the slow burst structure typical of our records near opposition, while Figure 3(*c*) shows the much faster modulation recorded nearer the Sun.

The curves in Figure 5 show how the velocity component, which is responsible for sweeping the diffraction pattern across the Earth, changes as a function of Jupiter's elongation and the distance to the diffracting layer. In general, V_p increases as the line of sight to Jupiter approaches the Sun, with the result that the burst rate should also increase. At elongations in the range $20° < \epsilon < 60°$, depending on the distance to the diffracting screen, the transverse component of velocity will reach a maximum value and then decrease rather rapidly. However, the r.m.s. phase deviation introduced at decametric wavelengths may be increasing so rapidly that the diffraction scale length on the ground is becoming significantly smaller, according to equation (9) of Section IV; this effect would largely compensate for the decrease in V_p, with the result that the burst rate would probably continue to increase until the angular separation was only a few degrees.

The results plotted in Figure 6 agree qualitatively with the predictions of the simple radial model of the solar wind. Unfortunately, the relatively long response time of the recorder pen probably results in an underestimation of the burst rates at elongations less than $\sim 50°$. In addition, a legitimate comparison cannot be made with the curves of Figure 5 close to opposition or conjunction because of the known small defects in the geometry that was assumed in drawing these curves. In the range of elongations $70° < \epsilon < 160°$, in which the measurements are reliable and the geometrical defects play only an insignificant role, the results of Figure 6 could be fitted almost equally well by scaled versions of all of the curves in Figure 5; one such curve for a layer at 1 a.u. has been superimposed on Figure 6, and in what follows it will be assumed that it adequately represents the average burst rate over this restricted range of elongations.

The dispersion in the measured burst rates may be due to one or more of the following causes: (1) errors in counting bursts, (2) bursts on different nights may originate in thin diffraction screens situated at different distances along the line of sight, and (3) temporal changes in the velocity of the solar wind. The scatter of points in Figure 6 about the dashed curve possesses an r.m.s. value of $\sim 20\%$, which is much higher than the r.m.s. uncertainty of $\sim 4\%$ assigned to each estimate on the basis of measurement error. Consequently, the major source of dispersion is probably to be found in (2) or (3).

The effect of (2) is considerably reduced by the magnification factor $(Z_1+Z_2)/Z_2$, which acts to oppose the influence of the changing transverse component of velocity V_p as the distance to the diffracting screen Z_1 is varied. This process is so effective that an r.m.s. dispersion of $\sim 20\%$ from (2) could result only if the diffraction peaks originate in relatively thin screens that assume different positions from night to night over almost the complete path between Jupiter and the Earth. The focusing conditions specified by equation (8) in Section IV suggest that phase-changing screens with $\phi_0 \geqslant 1$ rad situated as close as 0·05 a.u. to the Earth or Jupiter would produce the observed high degree of intensity modulation. However, it seems more likely that interplanetary space is filled with a continuous distribution

of scattering irregularities; as a result, the velocity dispersion due to (2) would be considerably lower than 20%.

A more likely origin for the dispersion in burst rate seems to be (3). Fluctuations in the magnitude of the solar wind with r.m.s. value of 20% averaged over the significant diffracting path would account for the results. Alternatively, r.m.s. angular deviations of a few degrees in the direction of the solar wind would also be effective.

Measurements by spacecraft of plasma velocities in the interplanetary medium near the Earth have shown a marked dependence on the degree of solar activity, the correlation with the K_p magnetic index being especially well developed. For the Jovian burst rate observations, many of the results relate to those parts of the interplanetary medium at appreciable distances from the Sun–Earth line; in these circumstances the K_p index may not be a suitable quantity with which to correlate our measurements of burst rate. Indeed, there appears to be no general correlation with either the K_p index or sunspot number in the comparatively few measurements of burst rate available to us. However, the most extreme deviation of +175% from the average burst rate was measured at a time of high geomagnetic and solar activity; this occurred on September 14, 1963 during strong Jovian emission in the interval 15^h17^m to 15^h47^m U.T. The rather high Jovian elongation of 155° probably ensured that the K_p index gave a reasonable indication of the magnetic disturbance in the diffracting region; accordingly, we suggest that the coincidence was not accidental, because both the Jovian burst rate and geomagnetic activity were exceptional events.

VII. Scale of Diffraction Patterns

In Section IV the spatial autocorrelation function has been defined by the Gaussian function

$$\rho(\xi) = \exp(-\xi^2/\xi_0^2),$$

where $\xi = \xi_0$, the distance along the ground for which the correlation has been reduced to $\exp(-1)$, is defined as the scale length. There are, in fact, various scale lengths corresponding respectively to the variations in complex amplitude, amplitude, intensity (amplitude squared), and phase. Cross-correlation of the post-detector outputs of spaced receivers yields estimates of the scale length of the amplitude or intensity variations. The method of the drifting pattern provides similar information. Phase-sensitive interferometers, on the other hand, measure the scale length of the complex amplitude variations, which include the effects of both amplitude and phase. There is no *a priori* reason for assuming that the various scale lengths are identical, especially in the case of a thick diffracting region that produces relatively strong phase deviations.

(a) *Cross-correlation of Post-detector Recordings*

This type of analysis results in a measure of the drift velocity of the diffraction pattern as well as providing information on the spatial autocorrelation of intensity.

Unfortunately, the method is not easy to apply to the analysis of pen recordings; in addition, it is of doubtful value in the presence of ionospheric scintillations, which often appeared to be affecting our observations. With these disadvantages in mind, it was not considered fruitful to compute the cross-correlation coefficients between total power recordings. However, many recordings taken over the 85·5 and 200 km baselines in the three months near opposition showed a reasonable degree of similarity between the bursts at the spaced sites. Thus it appears likely that the scale lengths associated with the intensity variations are of the order of hundreds of kilometres.

(b) *Method of the Drifting Pattern*

It was shown in Section IV that the average scale length of the intensity variations across the plane perpendicular to the line of sight is given by

$$\xi_0 = (2\cdot6)^{-1}\,\bar{V}_p'\,\bar{\tau},$$

where ξ_0 is the scale length of a Gaussian autocorrelation function, $\bar{V}_p'$ is the average velocity of the diffraction pattern, and $\bar{\tau}$ is the average interval between the arrival of diffraction peaks. Using this method the scale lengths have been calculated on the 10 occasions for which the pattern velocities were computed from the differences in burst arrival time. The more accurate values of ξ_0 listed in column 7 of Table 2 possess random errors with an r.m.s. value of about 30%, although there may well be some additional systematic error (e.g. the very high value for ξ_0 on October 29, 1964 is believed to be influenced by the systematic error in $\bar{V}_p'$ discussed in Section V). The average of the five most reliable estimates in Table 2 is $[\xi_0]_{av} = 380$ km, a value that is consistent with the high degree of correlation seen on our total power recordings over the 200 km baseline on a few occasions.

(c) *Measurements of Angular Power Spectrum*

Equations (5) and (6) of Section IV show that measurements of the angular power spectrum of the scattered radiation by a phase-sensitive interferometer provide estimates of the scale length of the complex amplitude variations across the plane perpendicular to the line of sight. In interpreting our measurements of fringe visibility, we have assumed that the scattering is strong enough to ensure that practically all of the radiation incident on the layer has been scattered into an angular power spectrum whose half-width to exp(−1) is given by equations (6). It will be shown in Section VIII that the phase modulation at 19·7 MHz is strong enough to ensure that this assumption is valid.

The angular size measurements have already been described by Slee and Higgins (1966), but in Figure 7 the information is presented in the form of a histogram in which the abscissae can be interpreted as either an angular size or a scale length. All the results in Figure 7 come from noise storms recorded when Jupiter's elongation exceeded 79°; interferometer fringes observed at lower values of elongation in 1964 were not adequately calibrated. An inspection of Figure 7 reveals that the majority of the measurements of scale length fell in the range $130 < \xi_f < 190$ km, values that are significantly lower than the intensity scale length derived from the method

of the drifting pattern. This interesting difference in the scale lengths of the intensity and complex amplitude patterns may well be a consequence of the long diffracting path through the interplanetary medium. The implications of such an interpretation are left to the discussion in Section IX.

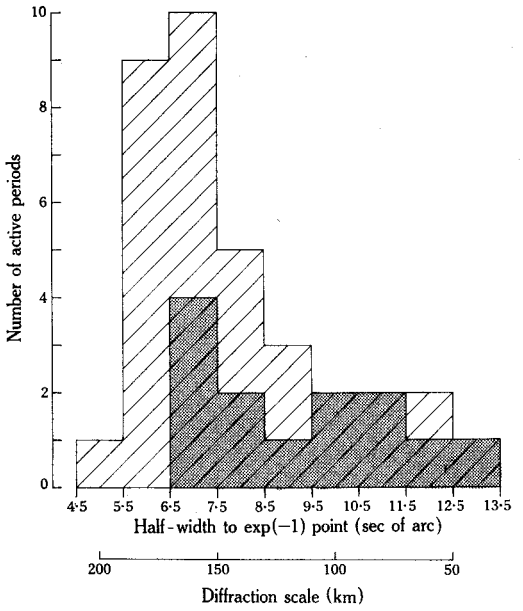

Fig. 7.—Histograms showing the distributions of half-widths in the angular power spectra of the scattered radiation at 19·7 MHz, deduced from measurements of interferometer fringe visibility. The shaded and hatched areas refer respectively to the results from 1963 and 1964. A second set of abscissae transforms the half-widths to the equivalent scale lengths in the complex amplitude variations across the ground.

VIII. Phase Deviations

Despite the limitations imposed upon 20 MHz interferometer observations by the phase stability of the Earth's ionosphere, recordings such as that shown in Figure 3(*a*) demonstrate that meaningful angular position measurements can be made for periods up to several minutes in duration. For these measurements, we are primarily interested in the relative positions of the fringe crossover points on the phase-sensitive recordings, since these are the only times at which the phase differences between the Jupiter signals at the spaced receiving sites are sampled.

Our method of measuring the phase deviations was determined by the fact that measurable fringes were normally recorded in groups with durations ranging from about 10 to 60 sec; each group or sample contained between 3 and 12 fringes. We computed the average fringe period for each sample and compared it with the expected period based on the hour angle and declination of Jupiter and the baseline parameters. This comparison resulted in obtaining: firstly, the fractional deviation of each sample mean from the theoretical period $\Delta T/T$; and secondly, the average fractional deviation of the individual crossover positions within each sample from their unperturbed positions, $n^{\frac{1}{2}}(\Delta T/T)$, in which n is the number of fringes in the sample. The latter calculation assumes that the diffraction peaks were frequent enough to ensure randomization from fringe to fringe, a condition almost certainly

fulfilled by these observations. Lastly, it was then an easy matter to compute the r.m.s. phase deviations between the ends of the baseline from the relation

$$\{\overline{(\Delta\phi)^2}\}^{\frac{1}{2}} = 1{\cdot}25\, n^{\frac{1}{2}}(\Delta T/T)\, 2\pi,$$

where 1·25 is the factor by which the r.m.s. deviation of a Gaussian distribution exceeds the mean deviation.

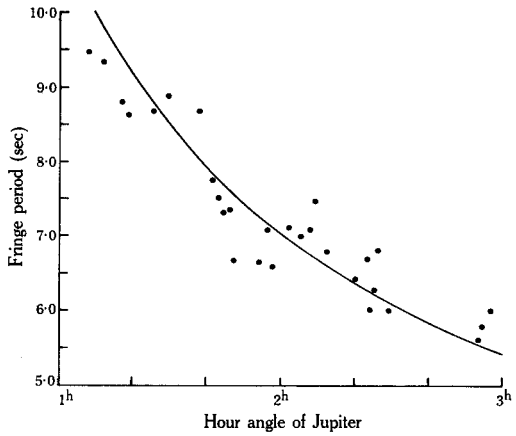

Fig. 8.—The interferometer fringe periods plotted against Jovian hour angle. Each point represents the average period in a sample of several fringes. The curve shows the expected fringe period calculated from the baseline parameters.

Some of the observational material from which the phase deviations were obtained is shown in Figure 8, where the fringe sample periods are plotted as a function of hour angle for a noise storm recorded on the 85·5 km baseline; the theoretical fringe period curve is superimposed on the figure. It is apparent that the points are distributed about the curve in a manner to be expected of sample periods that are being affected by random phase deviations.

Ionospheric scintillations are unlikely to have invalidated these measurements of phase for the reasons: (1) Except for low values of Jovian elongation, most fringes were recorded when the bursts at the separated sites showed a reasonable degree of correlation, indicating that scintillations at either site were not severe. (2) Many of the fringe samples were of durations less than 20 sec, which is considerably shorter than the time scale of most scintillations; consequently, the full effect of their associated phase deviations should not be felt. (3) The results in Figure 10 show that near opposition, when the Jovian radiation was recorded in the interval of maximum ionospheric scintillation activity, 2300 to 0200 hr local time, the measured phase deviations were comparatively low; on the other hand, the high r.m.s. phase deviations observed at Jovian elongations less than 40° were recorded just before local dawn when severe ionospheric scintillations are virtually absent.

The influence of the interplanetary medium on the phase deviations is shown in Figure 9, which contains histograms of the distribution of the quantity $\Delta T/T$ for all fringe samples recorded in 1963 and 1964. In order to construct these diagrams, the observations have been subdivided into three approximately equal numbers of fringe samples corresponding to the ranges of Jupiter's elongation $26° < \epsilon < 120°$,

$120° < \epsilon < 150°$, and $150° < \epsilon < 180°$. It is obvious that the fringe periods show a much larger dispersion about the theoretical values at the lower elongations.

A more detailed impression of the pronounced variation in the strength of the phase fluctuations on the ground is obtained from Figure 10. The data for this figure were obtained by averaging the r.m.s. phase differences over intervals of 10° to 20° in Jovian elongation. Open and full circles refer respectively to the 200 and 85·5 km baselines.

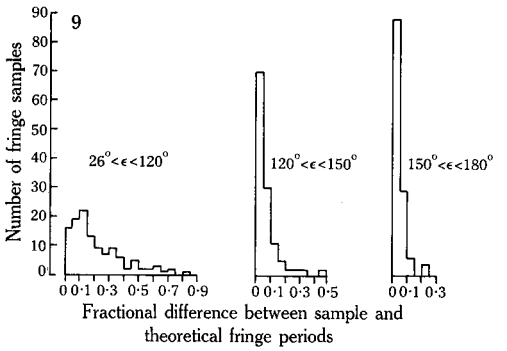

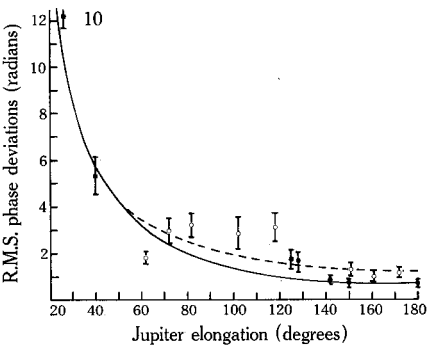

Fig. 9 (*left*).—Histograms of the deviations of the observed sample fringe periods from their unperturbed values for three ranges of Jovian elongation. Each deviation has been expressed as a fraction of the unperturbed fringe period.

Fig. 10 (*right*).—Estimates of the r.m.s. phase deviations between the ends of the baselines. Each point is an average of phase measurements made during several successive active nights. Full circles refer to 1963 measurements, 85·5 km baseline; full squares to 1964 measurements, 85·5 km baseline; open circles to 1964 measurements, 200 km baseline. The solid and dashed curves are respectively the r.m.s. phase differences over the 85·5 km and 200 km baselines predicted by a simple model for the scattering irregularities described in the text.

The curves superimposed on Figure 10 show the r.m.s. phase differences that would be measured over each baseline if the electron irregularities in the solar wind satisfied a model with the following characteristics: (1) The r.m.s. fluctuation in electron density near the ecliptic varies with heliocentric distance as R^{-2} and the irregularities possess a scale size that is substantially constant throughout the interplanetary medium. This assumption allows the form of the integral expression for the r.m.s. phase modulation $\phi_0(\epsilon)$ given by equation (4) in Section IV to be determined. (2) The phase fluctuations across the ground possess a Gaussian autocorrelation function and, at opposition, the scale length ξ_ϕ equals the irregularity scale in the scattering medium, L, which is assumed to be 150 km; at other elongations $\xi_\phi = L/\phi_0$. The latter condition is equivalent to specifying that $\phi_0 = 1$ rad at opposition. With ϕ_0 and ξ_ϕ determined at all elongations, equation (7) in Section IV has been used to derive $\{\overline{(\Delta\phi)^2}\}^{\frac{1}{2}}$ as a function of Jovian elongation for each of the baselines used in the experiment.

It is apparent from Figure 10 that the measured values of $\{\overline{(\Delta\phi)^2}\}^{\frac{1}{2}}$ are in reasonable agreement with the proposed model, particularly at the low and high values of elongation. In a sense, the curves have been forced to fit the observations at opposition by assuming a value for ϕ_0 that would produce the observed phase

differences. However, the consistent difference between the results for the two baselines over the range of elongations $140° < \epsilon < 180°$ may be used to independently assess the agreement between the observations and the proposed model. The measurements in the range of elongations $80° < \epsilon < 130°$ suggest that either the model is not a particularly accurate one or the observations in this region are affected by some systematic source of error. The individual fringe samples contributing to these particular points yielded values of $\{\overline{(\Delta\phi)^2}\}^{\frac{1}{2}}$ showing a relatively large dispersion about the mean. Such behaviour would probably result from the influence of ionospheric scintillations, which would also systematically increase the observed r.m.s. phase differences.

Quite apart from the disturbing effects of ionospheric scintillations, it would be remarkable if observations taken over an interval of 16 months showed better agreement with the predictions of any simple model. Temporal changes in the properties of the solar wind would make it unlikely that a unique model for the scattering irregularities could be derived from these measurements. However, it is clear that these observations are at least consistent with the presence of scattering irregularities with an average scale size of ~ 150 km (similar to the scale derived from fringe visibility measurements) and with r.m.s. electron density varying approximately as the inverse square of the heliocentric distance. The r.m.s. phase modulation at $\epsilon = 180°$ is ~ 1 rad.

IX. Discussion of Results

The preceding sections have demonstrated that a slowly varying radio emission from Jupiter is often deeply modulated by interplanetary scintillations with quasi-periods of the order of seconds. In this section the observational results are used to deduce the physical properties of the solar wind and a comparison is made with the results of other experiments.

(a) *Velocity of Solar Wind*

The measurements of burst rate shown in Figure 6 demonstrate the presence of a radially directed outflow of scattering irregularities near the plane of the ecliptic. The comparatively few measurements of the time delay $\overline{\Delta t}$ between the arrival of bursts at spaced receivers suggest that the average velocity of the solar wind is ~ 600 km sec^{-1}. This result agrees well with the measurements of plasma velocity reported from the Mariner II experiments by Neugebauer and Snyder (1962). Information about the variability of the velocity has been deduced from the dispersion in burst rate; the results, which represent averages over considerable path lengths through the interplanetary medium, allow upper limits to be deduced for the variability in magnitude and direction of 20% and $\pm 5°$ respectively. In localized regions the variations may be much higher.

(b) *Scale of Irregularities in Solar Wind*

The results of Section VII show that the diffraction scale length of the intensity fluctuations across the ground is approximately 400 km; this may be compared with

the results of Douglas and Smith (1967), who derive a similar average scale size from their spaced-receiver observations. The scale length of the complex amplitude fluctuations is, however, significantly lower with a value of approximately 150 km; additional information from the angular position scintillations suggests that the scale length of the phase fluctuations across the ground is also of the order of 150 km. It therefore appears that the complex amplitude variations are largely in the form of phase fluctuations.

A plausible explanation of these results involves the presence of an extended diffracting medium in which the amplitude fluctuations are impressed on the radiation by phase irregularities at considerably greater distances than those that produce most of the phase fluctuations. Under these circumstances the scale length of the intensity fluctuations would be subjected to a larger magnification factor $(Z_1+Z_2)/Z_2$ than is applied to the phase scale.

An investigation of the integral equation (4) for the phase deviations, assuming that $\{\overline{(\Delta N)^2}\}^{\frac{1}{2}}$ varies as the inverse square of the heliocentric distance and L is constant, shows that near opposition $\sim 87\%$ of the total mean square phase deviation would be impressed on the radiation within a distance of 1 a.u. of the Earth. Nevertheless, the much weaker contributions to ϕ_0^2 from more distant irregularities could still give rise to appreciable intensity fluctuations if the total value of ϕ_0^2 is high enough. Without an adequate theory for the thick diffracting medium it is difficult to specify how the suggested spatial separation between regions producing intensity and phase deviations would be achieved. One plausible suggestion is that the intensity fluctuations that build up within the medium at some distance in front of the initial scattering irregularities are accompanied by apparent angular size increases, which eventually restrict the further growth of intensity modulation.

In any case, it is evident that the measurement of diffraction scale which takes account of the total phase modulation should be used to specify the scale length in the diffracting screen. Therefore, on the reasonable assumption that most of the phase modulation takes place within a distance of $Z_1 = 1$ a.u., the measurements of complex amplitude scale suggest that the irregularity scale in the solar wind is $L \sim 150$ km. This value agrees with the result of 143 km deduced by Hewish, Dennison, and Pilkington (1966) from studies of interplanetary scintillations from quasars at heliocentric distances of $\sim 0{\cdot}5$ a.u. There is therefore reasonable evidence that the scale of irregularities in the interplanetary medium remains approximately constant out to heliocentric distances of at least 1 to 2 a.u.

(c) *Electron Density in the Scattering Irregularities*

The measurements of angular scintillations have suggested that near opposition the value of ϕ_0 is approximately 1 rad; the rate of increase of ϕ_0 as the elongation decreases is consistent with a variation in r.m.s. electron density of the form

$$\{\overline{(\Delta N(R))^2}\}^{\frac{1}{2}} \sim \Delta N_0 R^{-2},$$

where R is the heliocentric distance and ΔN_0 is the r.m.s. electron density at $R = 1$ a.u. The irregularity scale in the solar wind is approximately constant with $L \sim 150$ km.

If this information is inserted in equation (4) and the integration performed with the limits appropriate to observations near opposition, the resulting equation can be solved for ΔN_0. The resulting expression for r.m.s. electron density is

$$\{\overline{(\Delta N(R))^2}\}^{\frac{1}{2}} \sim 0{\cdot}2\,R^{-2}.$$

The deduced value of $\Delta N_0 \sim 0{\cdot}2$ electrons cm^{-3} is an order of magnitude lower than the plasma densities measured by the spacecraft Mariner II in late 1962. Since the values obtained by the spacecraft were averages over volumes containing many scattering irregularities, it appears that the latter are rather weak fluctuations in the interplanetary plasma containing only about 10% of the total plasma density.

This computation of electron density agrees reasonably well with a result presented by Cohen *et al.* (1967), who used the variation in scintillation index of quasar 3C 273B at 430 MHz to derive the r.m.s. phase deviation ϕ_0 as a function of heliocentric distance. These authors also demonstrate that the r.m.s. electron density varies as the inverse square of the heliocentric distance, in agreement with the present conclusion.

(*d*) *Intrinsic Angular Dimensions of Jovian Decametric Sources*

The requirements to be satisfied by the angular size of a radio source if appreciable intensity fluctuations are observed on the ground plane are described by equation (10) in Section IV. The distance to the equivalent thin phase screen is not known with certainty, but it appears likely that near opposition $Z_1 \sim 2$ a.u. (based on the size of the intensity diffraction scale in relation to the phase scale on the ground). Hence, using $Z_1 = 2$ a.u. and $\xi_0 = 400$ km in equation (10), the angular radius of the Jovian decametric source is $< 0{\cdot}3$ sec of arc.

As the line of sight to Jupiter approaches closer to the Sun the r.m.s. phase modulation associated with the intensity fluctuations is likely to exceed 1 rad, so that the intensity scale length is reduced according to equation (9). This may eventually result in a reduction of the r.m.s. intensity fluctuation across the ground due to the failure of the source to satisfy the angular size criterion. Such effects on the scintillating radio sources have already been noted by Little and Hewish (1966), who have used the information to estimate angular size.

In order to ascertain whether the finite angular sizes of the Jovian sources are producing similar effects, an examination has been made of the extensive observations made with the Boulder decametric spectrograph covering the Jovian apparitions 1960 to 1966; these are reported by Warwick and Kreiss (1964) and Warwick and Dulk (1965, 1966). The analysis has been restricted to frequencies above 17·5 MHz, where ionospheric absorption and station interference are unlikely to be important factors.

Figure 11 shows the probability of reception of Jovian radio emission as a function of elongation; the figure also shows the fraction of noise storms classified as "smooth" or "weak", where these terms refer to the degree of fine structure in the intensity modulation with periods of a few seconds. The probability of detecting noise storms falls steadily from a maximum value of $\sim 0{\cdot}5$ near opposition to

$\sim 0{\cdot}15$ near the Sun, with a sudden marked reduction at elongations less than 60°. Figure 11 also shows clearly that the fine structure in the Jovian radiation virtually disappears at elongations less than 30°, although a marked reduction sets in well before at an elongation of about 60°.

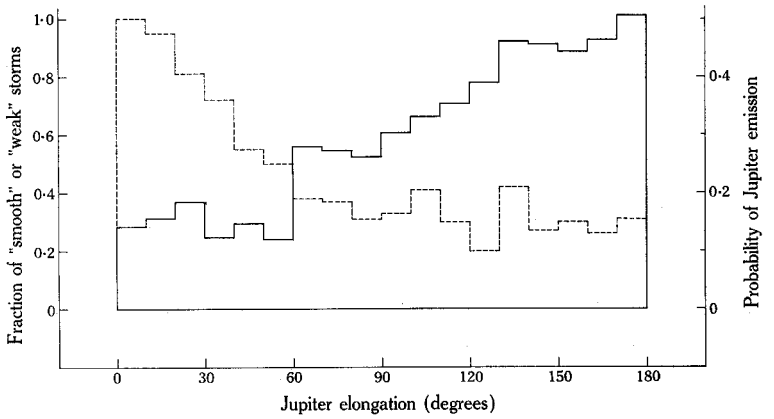

Fig. 11.—The full-line histogram (ordinate scale on right) is a plot of the probability of detection of Jovian emission $\geqslant 17{\cdot}5$ MHz as a function of Jovian elongation. The dashed-line histogram shows the "smoothness" (degree of very coarse time structure) present in the Jovian decametric emission plotted against elongation. (See text for further details.)

We suggest that the comparatively smooth intensity changes with periods of about 60 sec, which are recorded so often near the Sun, are the intrinsic changes in Jovian emission;* these can only be clearly distinguished when the short period modulation due to interplanetary scintillations has been removed by the failure of the source to satisfy the angular size criterion. The marked reduction in probability of reception of Jovian emission at the lower values of elongation is probably caused by difficulties in identifying the smooth emission, especially as it is usually of low peak intensity and partially obscured by interference and solar radio emission. The extension of the smooth emission into the antisolar region of elongations suggests that the angular dimensions of the Jovian sources may at times be large enough to ensure that the diffraction pattern is smoothed out, even with the comparatively weak scattering occurring near opposition.

If our explanation is correct, the finite angular sizes of the decametric sources are exerting a marked influence on the scintillation intensity at elongations $\leqslant 60°$. At $\epsilon = 60°$ the scale length of the intensity pattern is not known, but the poor correlation between total power recordings over our $85{\cdot}5$ km baseline at these low values of angular separation (see Fig. 3(*c*)) suggests that a value of $\xi_0 \sim 50$ km would be reasonable. The distance to the equivalent diffracting screen is assumed

* These slow intensity changes should not be confused with the modulation introduced by ionospheric scintillations. It can be demonstrated (see, for example, the grouping of Jovian bursts in Fig. 3(*d*)) that the radiation reaching the receiver almost always shows variability with a quasi-period of about 60 sec, even on those occasions when ionospheric scintillations are virtually absent.

to be $Z_1 \sim 1$ a.u. because, for these comparatively low elongations, the scattering will be strongest in this section of the ray path. Substitution of these values in equation (10) shows that the angular radius of the source is greater than 0·07 sec of arc. Hence the results shown in Figure 11 are consistent with a range of intrinsic angular radii given by $0{\cdot}07 < \psi_0 < 0{\cdot}3$ sec of arc; these values should be regarded as qualitatively correct, but they may need revision if the thin screen theory is shown to be inapplicable to decametric observations of Jupiter.

It appears reasonable to suppose that the effects caused by the finite angular size of the source at frequencies near 20 MHz would be even more developed at lower frequencies. Indeed, at frequencies of ~ 5 MHz it appears possible that intensity scintillation would not be severe at any Jovian elongation. In support of this suggestion, it should be noted that Ellis (1962) and Carr *et al.* (1965), both operating near 5 MHz, have pointed out the much smoother appearance of the Jupiter emissions at this frequency.

The well-known inverse correlation between general solar activity and frequency of reception of Jovian decametric radiation, first pointed out by Carr *et al.* (1961), may be yet another consequence of the finite source size. It is known from the measurements of the scattered angular power spectra from discrete radio sources near the Sun (Slee 1966) that the r.m.s. phase modulation introduced by the outer corona increases by a factor of about three from sunspot minimum to maximum. This increase would be sufficient to significantly reduce the degree of intensity scintillation over a large range of Jovian elongations, especially at the lower frequencies. It would be instructive to reassess the data on the "smoothness" of the Jovian emission as functions of wavelength, elongation, and sunspot cycle.

X. Acknowledgments

We wish to acknowledge the assistance of all those people who have contributed to the experiment in various ways. In particular, we thank Mr. C. F. Fryar and Mr. C. Tillack for help with the equipment and observations. We are indebted to the Postmaster-General's Department for allowing us to use the site and facilities at its radio-repeater station, Heaton. Our thanks are also due to the Electrical Engineering Department, University of Sydney, for permission to operate from the field station at Fleurs during 1964.

XI. References

Bramley, E. N. (1954).—*Proc. R. Soc.* A **225**, 515–18.

Bramley, E. N., and Young, M. (1967).—*Proc. Instn elect. Engrs* **114**, 553–6.

Burke, B. F., and Franklin, K. L. (1955).—*Nature, Lond.* **175**, 1074.

Carr, T. D., Gulkis, S., Smith, A. G., May, J., Lebo, G. R., Kennedy, D. J., and Bollhagen, H. (1965).—*Radio Sci.* **69D**, 1530–6.

Carr, T. D., Smith, A. G., Bollhagen, H., Six, N. F., and Chatterton, N. E. (1961).—*Astrophys. J.* **134**, 105–25.

Cohen, M. H., Gundermann, E. J., Hardebeck, H. E., and Sharp, L. E. (1967).—*Astrophys. J.* **147**, 449–66.

Douglas, J. N. (1964).—*IEEE Trans. Antennas Propag.* **AP-12**, 839–53.

DOUGLAS, J. N., and SMITH, H. J. (1961).—*Nature, Lond.* **192**, 741.
DOUGLAS, J. N., and SMITH, H. J. (1967).—*Astrophys. J.* **148**, 885–903.
ELLIS, G. R. A. (1962).—*Nature, Lond.* **194**, 667–8.
GARDNER, F. F., and SHAIN, C. A. (1958).—*Aust. J. Phys.* **11**, 55–69.
HEWISH, A., DENNISON, P. A., and PILKINGTON, J. D. H. (1966).—*Nature, Lond.* **209**, 1188–9.
LITTLE, L. T., and HEWISH, A. (1966).—*Mon. Not. R. astr. Soc.* **134**, 221–37.
NEUGEBAUER, M., and SNYDER, C. W. (1962).—*Science* **138**, 1095–6.
PISAREVA, V. V. (1958).—*Astr. Zh.* **35**, 112. (Translated in *Soviet Astr.* **2**, 97–111.)
RATCLIFFE, J. A. (1956).—*Rep. Prog. Phys.* **19**, 188–267.
SLEE, O. B. (1966).—*Planet. Space Sci.* **14**, 255–67.
SLEE, O. B., and GENT, H. (1967).—*Nature, Lond.* **216**, 235–8.
SLEE, O. B., and HIGGINS, C. S. (1963).—*Nature, Lond.* **197**, 781–3.
SLEE, O. B., and HIGGINS, C. S. (1965).—*Radio Sci.* **69D**, 1536–7.
SLEE, O. B., and HIGGINS, C. S. (1966).—*Aust. J. Phys.* **19**, 167–80.
SMITH, A. G., CARR, T. D., BOLLHAGEN, H., CHATTERTON, N., and SIX, F. (1960).—*Nature, Lond.* **187**, 568–70.
WARWICK, J. W., and DULK, G. A. (1965).—High Altitude Observatory, Boulder, IGY Solar Activity Report, Series No. 32.
WARWICK, J. W., and DULK, G. A. (1966).—High Altitude Observatory, Boulder, IGY Solar Activity Report, Series No. 34.
WARWICK, J. W., and KREISS, W. T. (1964).—High Altitude Observatory, Boulder, IGY Solar Activity Report, Series No. 28.